NANO LETTERS
Cite This: Nano Lett. XXXX, XXX, XXX−XXX
Letter
pubs.acs.org/NanoLett

Intervalley Scattering of Interlayer Excitons in a $MoS_2/MoSe_2/MoS_2$ Heterostructure in High Magnetic Field

Alessandro Surrente,[†] Łukasz Kłopotowski,[§] Nan Zhang,[†] Michal Baranowski,[†,∥] Anatolie A. Mitioglu,[⊥] Mariana V. Ballottin,[⊥] Peter C.M. Christianen,[⊥] Dumitru Dumcenco,[#,∞] Yen-Cheng Kung,[#] Duncan K. Maude,[†] Andras Kis,[#] and Paulina Plochocka*[,†]

[†]Laboratoire National des Champs Magnétiques Intenses, UPR 3228, CNRS-UGA-UPS-INSA, 38042/31400 Grenoble/Toulouse, France

[§]Institute of Physics, Polish Academy of Sciences, Al. Lotników 32/46, 02-668 Warsaw, Poland

[∥]Department of Experimental Physics, Faculty of Fundamental Problems of Technology, Wroclaw University of Science and Technology, 50-370 Wroclaw, Poland

[⊥]High Field Magnet Laboratory (HFML − EMFL), Radboud University, 6525 ED Nijmegen, The Netherlands

[#]Electrical Engineering Institute and Institute of Materials Science and Engineering, École Polytechnique Fédérale de Lausanne, CH-1015 Lausanne, Switzerland

[∞]Department of Quantum Matter Physics, Université de Genève, 24 quai Ernest Ansermet, CH-1211 Geneva, Switzerland

Supporting Information

ABSTRACT: Degenerate extrema in the energy dispersion of charge carriers in solids, also referred to as valleys, can be regarded as a binary quantum degree of freedom, which can potentially be used to implement valleytronic concepts in van der Waals heterostructures based on transition metal dichalcogenides. Using magneto-photoluminescence spectroscopy, we achieve a deeper insight into the valley polarization and depolarization mechanisms of interlayer excitons formed across a $MoS_2/MoSe_2/MoS_2$ heterostructure. We account for the nontrivial behavior of the valley polarization as a function of the magnetic field by considering the interplay between exchange interaction and phonon-mediated intervalley scattering in a system consisting of Zeeman-split energy levels. Our results represent a crucial step toward the understanding of the properties of interlayer excitons with strong implications for the implementation of atomically thin valleytronic devices.

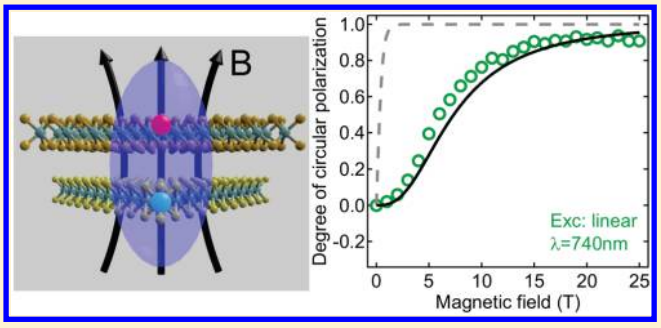

KEYWORDS: *Transition metal dichalcogenides, van der Waals heterostructures, interlayer exciton, magnetophotoluminescence, valley polarization*

In close analogy with spin and its use in quantum information processing,[1] the valley pseudospin[2] can potentially be used to encode, store, and transfer information. Although valley physics has been investigated in a variety of materials, including AlAs,[3] silicon,[4] diamond,[5] bismuth,[6] and graphene,[7] the lack of a direct band gap in these systems precludes optically addressing and reading out the valley degree of freedom. In monolayer transition metal dichalcogenides (TMDs), the valley degree of freedom corresponds to a direct band gap in the visible range at the nonequivalent but degenerate K^+ and K^- points of the Brillouin zone. This, along with the locking of the spin and valley degrees of freedom,[8] allows to optically initialize,[9] manipulate,[10] and read out[11] the valley pseudospin using circularly polarized light. The large exciton binding energy in these materials[12] is reflected in a very large dipole moment, which induces subpicosecond radiative lifetimes.[13] This, combined with very efficient intervalley scattering[14] mediated via electron−hole exchange interaction,[15] strongly limits the usefulness of monolayer TMDs in practical valleytronic devices for quantum information science.

A possibility to overcome these limitations is offered by van der Waals heterostructures, obtained by vertically stacking monolayers of different TMDs. Photoexcited charge carriers are quickly separated[16] due to the type II band alignment exhibited by heterobilayers,[17] forming a quasiparticle referred to as interlayer exciton. The spatial separation of the charges leads to a significant increase (up to 5 orders of magnitude, ∼100 ns) of the recombination lifetime of interlayer excitons.[18,19] Moreover, in analogy to intralayer excitons, valley polarization of interlayer excitons can be injected via optical excitation. The reduced

Received: April 13, 2018
Revised: May 14, 2018
Published: May 23, 2018

DOI: 10.1021/acs.nanolett.8b01484
Nano Lett. XXXX, XXX, XXX−XXX

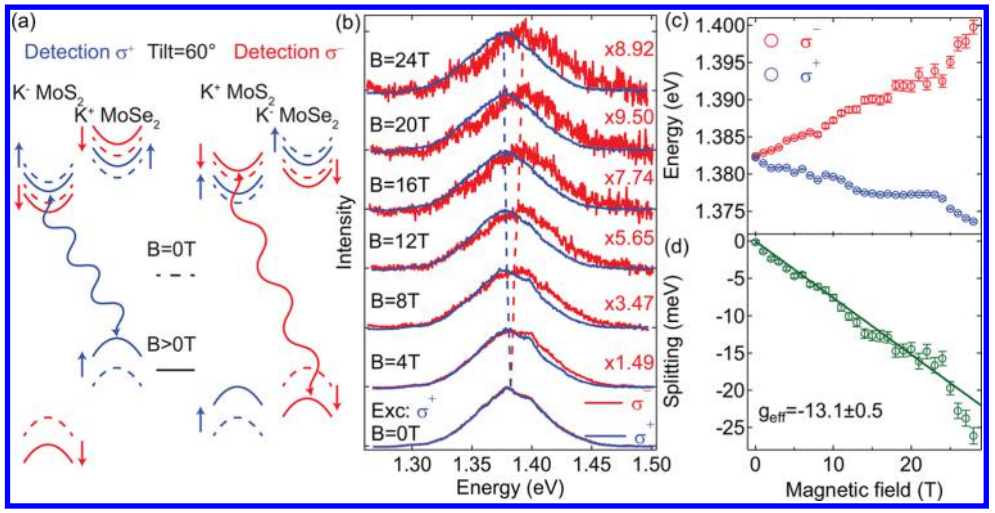

Figure 1. (a) Configuration of the relevant band edges at zero and high magnetic field, assuming a 60° stacking angle between the monolayers. The spin of the bands is color-coded and indicated by an arrow of the same color. Wavy arrows depict dipole-allowed optical transitions. (b) Interlayer exciton magnetoPL spectra up to 24 T. The spectra detected with σ^- polarization have been rescaled. The dashed lines are a guide for the eye. (c) Transition energies and (d) energy splitting of interlayer exciton as a function of magnetic field.

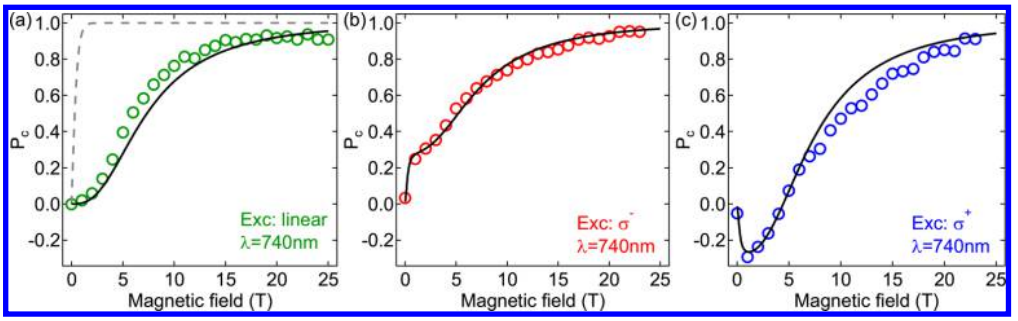

Figure 2. Magnetic-field dependence of P_c for (a) linearly polarized, (b) σ^- and (c) σ^+ polarized excitation. The dashed gray line shows the expected evolution of the circular polarization for an exciton population fully thermalized with the lattice. The measured circular polarization (symbols) is fitted with results of a four level rate equations model (lines).

spatial overlap of the electron−hole wave functions leads to a dramatically decreased electron−hole exchange interaction, which results in long-lived valley polarization (up to 40 ns).[20] These properties make interlayer excitons ideally suited for valleytronic applications.

The manipulation of the valley degree of freedom via the application of magnetic field has been successfully demonstrated for intralayer excitons.[21−25] This approach has recently been extended to interlayer excitons, where the observation of a giant valley Zeeman splitting and a subsequent near-unity valley polarization has been enabled by the 60° tilt angle between mechanically exfoliated $MoSe_2/WSe_2$ monolayers.[26] However, a fundamental understanding of the dynamics of the interlayer exciton population as well as valley depolarization mechanism is still lacking.

Here, we achieve a deeper insight into the properties of interlayer excitons by performing detailed magneto-photoluminescence (magnetoPL) spectroscopy of a heterostructure formed by MoS_2 and $MoSe_2$ monolayers.[19,27] The materials which compose our heterostructures are lattice mismatched. This leads to the formation of a moiré pattern,[28,29] which has been shown to influence the electronic and valley properties of interlayer excitons.[30−32] We lift the valley degeneracy by applying magnetic fields up to 28 T in the Faraday configuration. We observe a population imbalance in the Zeeman split valleys, which allows us to precisely control the valley polarization from 0 to almost 100% by applying the magnetic field. For the first time, we describe the magnetic field dependence of the valley polarization of a van der Waals heterostructure by a model, which accounts for the observed intervalley relaxation via an interplay between exchange and phonon driven intervalley scattering in Zeeman split levels.

The zero field PL and reflectivity contrast spectra of our structure are presented in the Supporting Information. The PL spectrum consists of sharp peaks attributed to the recombination of free and charged intralayer excitons in MoS_2 and $MoSe_2$,[27] and a low energy peak at ∼1.38 eV, which results from the radiative recombination of the interlayer exciton.[19] The red-shifted interlayer exciton in our heterostructure as compared to a mechanically exfoliated $MoS_2/MoSe_2$ bilayer deposited on SiO_2[33] could be partially attributed to the larger dielectric screening induced by sapphire. This is consistent with the trend observed in TMD monolayers when additional dielectric screening was purposefully introduced.[34] The magnetoPL is excited with circularly or linearly polarized light, and is detected using a circular polarization basis. A representative set of magnetoPL spectra of the interlayer exciton is presented in Figure 1b. The PL peak exhibits a significant Zeeman splitting and a considerable valley polarization, which increases with increasing magnetic field and saturates for $B > 20$ T. The slightly lower scaling factor for $B = 24$ T results from a small deviation from the saturated valley

DOI: 10.1021/acs.nanolett.8b01484
Nano Lett. XXXX, XXX, XXX−XXX

polarization reached at high fields due to experimental uncertainties (see, e.g., the valley polarization in Figure 2 and the valley polarization extracted from the data of Figure 1b shown in Figure S4c, Supporting Information). To analyze quantitatively our data, we fit a single Gaussian function to the PL spectra of the interlayer exciton and extract the emission energies, which are plotted in Figure 1c as a function of the magnetic field. The Zeeman shift of the σ^+ polarization is larger than that of the σ^- polarization. This is a consequence of the diamagnetic effect, quadratic in magnetic field, which blue shifts the exciton energy.[35] The observation of the diamagnetic shift reflects the relatively large electron hole separation and will be subject of a separate study. The energy difference between the two polarizations is shown in Figure 1d, where a very large valley Zeeman splitting of ∼25 meV at the highest magnetic field is observed. In analogy with the standard analysis for intralayer excitons, we define $\Delta E = E_{\sigma^+} - E_{\sigma^-} = g_{\text{eff}}\mu_B B$, where g_{eff} denotes the effective interlayer exciton g-factor, $\mu_B \sim 58$ μeV/T is the Bohr magneton, and B is the magnetic field. The fitting of the data of Figure 1d gives $g_{\text{eff}} = -13.1 \pm 0.5$. We estimated g_{eff} also with the center of mass method[22] (see Supporting Information for a more detailed discussion of the fitting procedures and for the corresponding plots), which yielded $g_{\text{eff}} = -13.4 \pm 0.5$, identical within experimental error to the value determined by fitting. This very large g_{eff} has been interpreted as stemming from a nonvanishing valley orbital contribution to the overall magnetic moments of the bands for heterostructures with a 60° stacking angle.[26] This configuration makes transitions between bands with different valley indexes optically bright, as shown in Figure 1a and discussed more in detail in the Supporting Information. In our heterostructure, the moiré pattern yields locally an AB configuration of the registry of the central $MoSe_2$ layer with one of the two MoS_2 layers, effectively similar to a lattice matched heterobilayer with 60° stacking angle. These spots are expected to be optically bright[31,32] and to exhibit a large Zeeman splitting, consistent with the data summarized in Figure 1. The smaller g_{eff} observed here, compared with that of a $MoSe_2/WSe_2$ heterostructure, is consistent with the smaller difference of the effective mass of the constituents of our sample.[36,37]

As seen in Figure 1b, applying a magnetic field results in a sizable difference of the PL intensities of the interlayer exciton recorded in σ^+ and σ^- polarizations. For a quantitative analysis, we define the degree of circular polarization as $P_c = (I^+ - I^-)/(I^+ + I^-)$, where $I^{\pm}$ denote the PL intensities in $\sigma^{\pm}$ polarizations, respectively. In Figure 2, we plot the magnetic field dependence of P_c for excitation in resonance with the A exciton of the $MoSe_2$ monolayer for (a) linear, (b) σ^-, and (c) σ^+ excitation polarization. In the case of intralayer excitons for an excitation with circularly polarized light, at $B = 0$ T we expect $P_c \neq 0$, which results from the optical orientation of the valley pseudospin.[9,38,39] This effect has been also observed in heterobilayers[20] and in our trilayer sample.[19] In Figure 2b,c, the observed optically oriented polarization at $B = 0$ T is very small, but it is recovered by applying a small field and already at 1 T $P_c \approx \pm 0.3$ for $\sigma^{\mp}$ excitation polarizations, respectively. The observed polarization is opposite to the polarization of the excitation beam, which is in agreement with our recent report.[19] This counterpolarized emission might be due to the effects of the moiré pattern, which only locally preserves the three-fold symmetry of the original crystals.[31,32] A local AB stacking (corresponding to a 60° stacking angle and consistent with the observations of Figure 1) represents a local potential minimum for the interlayer exciton, and it is characterized by a large oscillator strength of the interlayer exciton transition. It also couples to circularly polarized light of opposite helicity with respect to that of the excitation laser.[31,32] A possible explanation of the opposite polarization is that the optical excitation creates intralayer excitons in the monolayers. The charge carriers are rapidly separated,[16] forming interlayer excitons across the heterostructure, which relax to minima of the potential induced by the moiré pattern. These locations correspond to optically bright spots and couple primarily to light of opposite polarization.[31,32]

As the field is further increased, P_c increases and at $B > 20$ T reaches $P_c \approx 1$ regardless of excitation polarization. Nonzero P_c originates from an occupation difference between the interlayer exciton states in different valleys. In the following, we label these states as pseudospin up $|\uparrow\rangle$ and down $|\downarrow\rangle$, neglecting for the sake of simplicity the complicated spin/valley structure of the recombining interlayer exciton states depicted in Figure 1a. As the field is increased, the population imbalance increases due to the preferential occupation of the lower lying Zeeman state (the $|\uparrow\rangle$ state). If thermal equilibrium is established between the interlayer exciton system and the lattice, P_c is determined solely by the effective g-factor of the interlayer exciton and by the lattice temperature. The dashed line in Figure 2a shows the magnetic field dependence of this polarization, given by $P_c^{\text{eq}} = \tanh(\Delta E/(2k_B T))$, where ΔE is the Zeeman splitting between $|\downarrow\rangle$ and $|\uparrow\rangle$ states and $T = 4.5$ K is the bath temperature. The discrepancy between the experimental results shown in Figure 2a and P_c^{eq} visible at $B \lesssim 15$ T suggests that either the equilibrium is not established or the interlayer exciton system is characterized by a spin temperature significantly larger than 4.5 K. Even though the interlayer exciton energy (and/or its g-factor) suffers from inhomogeneous broadening, we find its impact negligible on the expected equilibrium P_c.

In order to determine the underlying relaxation processes responsible for the observed field dependence of P_c, we employ a four-level rate equation model[40,41] depicted schematically in Figure 3 (see Supporting Information for further details). The solution of this model provides the field dependence of the interlayer exciton populations $n_\uparrow$ and $n_\downarrow$ of the Zeeman split $|\uparrow\rangle$

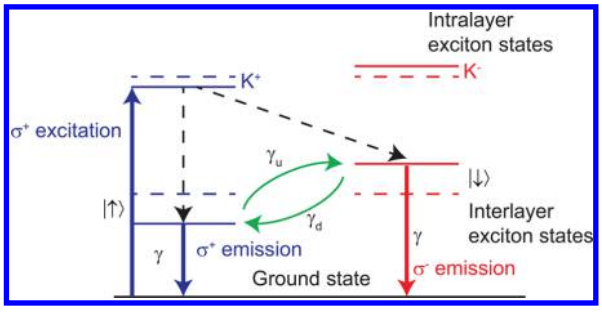

Figure 3. Schematic of the rate equations model for the case of σ^+ excitation. Dashed and solid horizontal lines denote the relevant exciton states at $B = 0$ T and at $B > 0$ T, respectively. A laser beam creates excitons in K^+ valley of one of the constituent monolayers. The type-II band alignment in the heterostructure leads to an ultrafast charge separation and formation of an interlayer exciton. This process is denoted by dashed arrows. The recombination of the interlayer exciton, denoted by thick, straight arrows, occurs with a rate γ and competes with intervalley scattering, denoted by curved thin arrows, occurring with rates γ_u and γ_d for the scattering upward and downward in energy, respectively.

DOI: 10.1021/acs.nanolett.8b01484
Nano Lett. XXXX, XXX, XXX−XXX

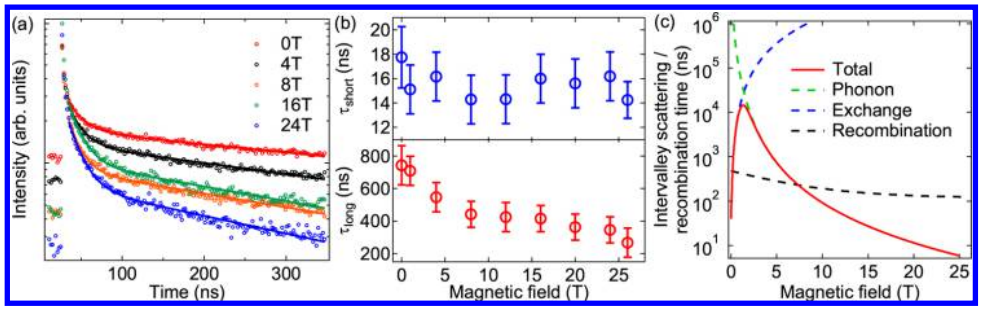

Figure 4. (a) Temporal decays of the interlayer exciton PL for various magnetic fields plotted together with fitted biexponential decay functions. (b) Magnetic field dependence of the short and long decay times. (c) Comparison between the intervalley scattering time τ_v and the recombination time τ_{avg}. The contributions to the intervalley scattering from the exchange-driven process and the spin−lattice relaxation process are also shown. τ_{avg} is interpolated from the measured PL decay times.

and $|\downarrow\rangle$ states. Assuming that $P_c = (n_\uparrow - n_\downarrow)/(n_\uparrow + n_\downarrow)$, we find[40,41]

$$P_c = P_0 \frac{\gamma}{\gamma + \gamma_d + \gamma_u} + \frac{\gamma_d - \gamma_u}{\gamma + \gamma_d + \gamma_u} \quad (1)$$

where $\gamma_{u,d}$ are intervalley scattering rates (see Figure 3) and γ denotes the recombination rate. The first term describes the optically created polarization in which P_0 is the polarization transferred from the circularly polarized excitation. The second term describes the tendency of the system to reach thermal equilibrium. The intervalley scattering rates can be written as[42,43]

$$\gamma_{u,d} = \frac{1}{\tau_{v0}} \frac{\Gamma^2}{\Gamma^2 + \Delta E^2} + \frac{\alpha \Delta E^3}{\left| \exp\left(\frac{\pm \Delta E}{k_B T}\right) - 1 \right|} \quad (2)$$

where the first term describes the effect of the electron−hole exchange interaction, which acts as an effective in-plane magnetic field on the valley pseudospin with a zero-field intervalley relaxation time τ_{v0}. The precession of the valley pseudospin around this effective field, together with the reorientation of this field due to momentum scattering,[44] induces the intervalley scattering. However, this is a zero-energy process and thus it is only efficient when the two valley states $|\uparrow\rangle$ and $|\downarrow\rangle$ are close in energy. Therefore, this resonant process is controlled by the width parameter Γ. As the Zeeman splitting ΔE is increased, the exchange-driven relaxation slows down and becomes negligible when the field-induced splitting ΔE becomes much larger than Γ. The second term in eq 2 describes the one-phonon spin−lattice relaxation process,[45] which requires the emission or absorption of a phonon, if the scattering occurs to the lower (γ_d) or higher (γ_u) valley, respectively. Consequently, the scattering rates are proportional to the phonon Bose occupation factors $n_k + 1$ or n_k, respectively. In eq 2, α is a measure of the exciton−phonon coupling strength, independent of ΔE.

We evaluate experimentally the recombination rate γ by measuring the time-resolved PL of the interlayer exciton. The temporal decays of the PL signal are shown in Figure 4a. The PL decays are fitted well with a biexponential function. The short decay time obtained from the fitting, τ_{short}, presented in Figure 4b, is about 16 ns, and insensitive to the magnetic field. The fitted long decay time, τ_{long}, as shown in Figure 4b, decreases from about 700 to 350 ns over the investigated field range. In agreement with previous reports,[18,19] both decay times are 3−5 orders of magnitude longer than the decay of excitonic PL from a monolayer, a consequence of the spatial separation of the electron-hole pairs. The shortening of τ_{long} with increasing magnetic field can be attributed to the magnetic field induced shrinking of the exciton orbital wave function.[46] Because of the small time window of 350 ns available to detect the PL in these experiments, the evaluation of the long decay time is subject to significant errors.

For the purpose of fitting the field dependence of P_c with our model calculations, we define the average decay time as $\tau_{avg} = (A_{long}\tau_{long} + A_{short}\tau_{short})/(A_{long} + A_{short})$, where A_{long} and A_{short} are the amplitudes of the long and short decays, respectively, and assume that $\gamma = 1/\tau_{avg}$. To obtain γ for all the fields at which P_c was recorded, we interpolate the field dependence of τ_{avg} with an exponential function (see Supporting Information).

The fitting of the model is performed globally to the three sets of data presented in Figure 2a−c. The fitting parameters are τ_{v0}, Γ, α, and the transferred polarization $P_0 = 0$ for linear excitation and $\mp P_0$ for σ^+ and σ^- excitations, respectively. The agreement between the fitted curves (solid lines in Figure 2a−c) and the experimental data is very good, which allows us to reconstruct the field-induced changes of the intervalley scattering rates. At fields $\ll$1 T, the optically created valley polarization is quenched by the exchange-driven process.[44] In TMD monolayers, this process leads to intervalley scattering times of the order of a few picoseconds.[14] In heterostructures, due to the spatial separation of the electron and the hole the efficiency of this process is dramatically reduced. The zero-field intervalley relaxation time obtained from our fitting is $\tau_{v0} = 40$ ns, 4 orders of magnitude larger than that of excitons in a WSe_2 monolayer[14] and similar to the values reported for a WSe_2/$MoSe_2$ heterostructure.[20] As the field is increased up to ~5 T, the exchange-driven mechanism is suppressed and the optically created polarization is recovered. Thus, for $\sigma^\pm$ excitations P_c becomes negative or positive, respectively, and our fitting yields $P_0 = \mp 0.29$. The value of Γ obtained from the fitting is 40 μeV. This value is much smaller than the line width of the interlayer transition, which suffers from a strong inhomogeneous broadening, possibly induced also by the laterally varying distance between the monolayers constituting the heterostructure and resulting from residual adsorbates between them. Also, the obtained Γ is smaller than the exciton homogeneous line width measured for monolayer WSe_2.[13] A similar recovery of the optically created valley polarization was observed for long-lived localized excitons in monolayer tungsten dichalcogenides.[47] The recovery was attributed to a suppressed intervalley scattering of dark excitons. This mechanism might contribute to the recovery of the polarization in our heterostructure, given that the optically active AB stacking

DOI: 10.1021/acs.nanolett.8b01484
Nano Lett. XXXX, XXX, XXX−XXX

mimics the band structure of W-based TMDs, with dark exciton states lying energetically below the bright ones.[48] The recovery of P_c at small fields suggests that the spin−lattice relaxation is slower than the recombination in this magnetic field range, which leads to a nonequilibrium occupations of the interlayer exciton states. As the field is increased above ∼5 T, the rate of spin−lattice relaxation increases and drives the system toward equilibrium. Our model assumes that for $\Delta E \gg k_B T$, the intervalley scattering rate increases as ΔE^3. When this rate becomes larger than γ, the P_c becomes positive and no longer determined by the excitation polarization. Our fitting yields α = 5 ns^{-1} eV^{-3}. A very similar value was obtained for excitons in GaAs quantum wells,[43] which is a surprising coincidence because we would expect a stronger exciton−phonon coupling in TMDs.[13]

Using eq 2 and our fitted parameters, we calculate the field dependence of the intervalley scattering time as $\tau_v = 1/(\gamma_d + \gamma_u)$ and compare it to the interpolated average recombination time τ_{avg} in Figure 4c. As inferred from the analysis of the evolution of P_c with magnetic field, $\tau_v < \tau_{avg}$ at $B < 1$ T, where the exchange-driven process dominates. Then, in the intermediate field range 1 T $\leq B \lesssim$ 7 T, τ_v becomes larger that τ_{avg}. Above ∼7 T, the intervalley scattering time decreases below the recombination time due to the increased Zeeman splitting ΔE, and the interlayer exciton system is driven toward thermal equilibrium, as evidenced by the experimental data which approach the dashed curve in Figure 2.

In conclusion, we have performed detailed magnetoPL spectroscopy of interlayer excitons formed in a $MoS_2/MoSe_2/MoS_2$ heterostructure. The effective g-factor of the interlayer exciton is significantly larger as compared to that of intralayer excitonic transitions, due to a nonvanishing contribution of the valley orbital moments. The large electron−hole separation in the interlayer exciton results in the suppression of intervalley scattering, which is directly reflected in our polarization-resolved measurements. At zero magnetic field, the polarization degree is mainly determined by the intervalley scattering driven by the electron−hole exchange interaction. A small magnetic field can efficiently suppress this mechanism, which results in the recovery of the optically induced polarization. In the high-field limit, the PL polarization is dominated by the thermal occupation of Zeeman split states and does not depend on the injected polarization. The interplay between exchange interaction, phonon driven scattering, and magnetic field can result in nonmonotonic behavior of the valley polarization. Our results represent a crucial step for the implementation of valleytronic concepts based on interlayer excitons by providing a thorough insight into the valley polarization generated via an applied magnetic field and the competing depolarization mechanisms.

Methods. *Sample Preparation.* Large area MoS_2 and $MoSe_2$ monolayer films, which form the investigated heterostructure, were grown separately by chemical vapor deposition (CVD) on sapphire substrates.[49,50] The heterostructure was fabricated by two sequential KOH-based transfer steps.[51] The first transfer allowed the formation of a $MoS_2/MoSe_2$ heterobilayer, which was subsequently transferred onto a MoS_2 film to form the trilayer stack.[27] This approach allowed us to obtain multiple van der Waals heterostructures with varying stacking angles over very large areas.[19,27]

Magneto-Optical Spectroscopy. The sapphire substrate with large area heterostructures was mounted on a $x-y-z$ translation stage driven by piezoelectric actuators and cooled down at 4.5 K in a liquid helium cryostat. Static magnetic fields up to 28 T were applied making use of a water-cooled resistive magnet. The PL was excited by a diode laser emitting at 640 nm (excitation in resonance with the MoS_2 A exciton) or a Ti:sapphire laser tuned at 740 nm (excitation in resonance with the $MoSe_2$ A exciton). The typical excitation power was kept as low as possible and in any case lower than 30 μW. The excitation laser was circularly or linearly polarized with a linear polarizer and a Babinet-Soleil compensator. The beam was focused on the sample by a long working distance microscope objective, which was also used to collect the PL. This signal was analyzed in a circular polarization basis with a zero-order quarter-waveplate and a linear polarizer and dispersed by a 0.3 m long monochromator coupled to a liquid nitrogen-cooled charge-coupled device detector. Time-resolved magnetoPL was measured by operating the diode laser in pulsed mode with a repetition frequency of 2.5 MHz, synchronized with a Si avalanche photodiode. The PL was spectrally selected by making use of a long-pass filter.

■ ASSOCIATED CONTENT

Supporting Information

The Supporting Information is available free of charge on the ACS Publications website at DOI: 10.1021/acs.nanolett.8b01484.

Low-temperature μPL spectra of a $Mo_2/MoSe_2/MoS_2$ heterostructure at zero magnetic field, estimation of valley Zeeman splitting for intralayer and interlayer excitons, additional details concerning the fitting procedures used for the determination of the PL energy, four level rate equation model and magnetic field dependence of the valley polarization for an excitation in resonance with the A exciton of MoS_2 (PDF)

■ AUTHOR INFORMATION

Corresponding Author

*E-mail: paulina.plochocka@lncmi.cnrs.fr.

ORCID

Alessandro Surrente: 0000-0003-4078-4965
Łukasz Kłopotowski: 0000-0001-8327-2156
Andras Kis: 0000-0002-3426-7702
Paulina Plochocka: 0000-0002-4019-6138

Notes

The authors declare no competing financial interest.

■ ACKNOWLEDGMENTS

This work was partially supported by the Région Midi-Pyrénées under contract MESR 13053031, BLAPHENE, and STRABOT projects, which received funding from the IDEX Toulouse, Emergence program, by "Programme Investissements d'Avenir" under the program ANR-11-IDEX-0002-02, reference ANR-10-LABX-0037-NEXT and by the PAN−CNRS collaboration within the PICS 2016-2018 agreement. N.Z. holds a fellowship from the Chinese Scholarship Council (CSC). This work was also financially supported by the Swiss SNF Sinergia Grant 147607. M.B. acknowledges support from Polish Ministry of Higher Education and Science through Grant DEC 1648/MOB/V/2017/0. This work was also supported by HFML-RU/FOM and LNCMI-CNRS, members of the European Magnetic Field Laboratory (EMFL).

DOI: 10.1021/acs.nanolett.8b01484
Nano Lett. XXXX, XXX, XXX−XXX

REFERENCES

(1) Awschalom, D. D.; Bassett, L. C.; Dzurak, A. S.; Hu, E. L.; Petta, J. R. Quantum spintronics: engineering and manipulating atom-like spins in semiconductors. *Science* **2013**, *339*, 1174−1179.

(2) Xu, X.; Yao, W.; Xiao, D.; Heinz, T. F. Spin and pseudospins in layered transition metal dichalcogenides. *Nat. Phys.* **2014**, *10*, 343−350.

(3) Shkolnikov, Y.; De Poortere, E.; Tutuc, E.; Shayegan, M. Valley splitting of AlAs two-dimensional electrons in a perpendicular magnetic field. *Phys. Rev. Lett.* **2002**, *89*, 226805.

(4) Salfi, J.; Mol, J.; Rahman, R.; Klimeck, G.; Simmons, M.; Hollenberg, L.; Rogge, S. Spatially resolving valley quantum interference of a donor in silicon. *Nat. Mater.* **2014**, *13*, 605.

(5) Isberg, J.; Gabrysch, M.; Hammersberg, J.; Majdi, S.; Kovi, K. K.; Twitchen, D. J. Generation, transport and detection of valley-polarized electrons in diamond. *Nat. Mater.* **2013**, *12*, 760−764.

(6) Zhu, Z.; Collaudin, A.; Fauqué, B.; Kang, W.; Behnia, K. Field-induced polarization of Dirac valleys in bismuth. *Nat. Phys.* **2012**, *8*, 89−94.

(7) Gorbachev, R.; Song, J.; Yu, G.; Kretinin, A.; Withers, F.; Cao, Y.; Mishchenko, A.; Grigorieva, I.; Novoselov, K.; Levitov, L.; Geim, A. Detecting topological currents in graphene superlattices. *Science* **2014**, *346*, 448−451.

(8) Xiao, D.; Liu, G.-B.; Feng, W.; Xu, X.; Yao, W. Coupled spin and valley physics in monolayers of MoS_2 and other group-VI dichalcogenides. *Phys. Rev. Lett.* **2012**, *108*, 196802.

(9) Mak, K. F.; He, K.; Shan, J.; Heinz, T. F. Control of valley polarization in monolayer MoS_2 by optical helicity. *Nat. Nanotechnol.* **2012**, *7*, 494−498.

(10) Ye, Z.; Sun, D.; Heinz, T. F. Optical manipulation of valley pseudospin. *Nat. Phys.* **2016**, *13*, 26−29.

(11) Hao, K.; Moody, G.; Wu, F.; Dass, C. K.; Xu, L.; Chen, C.-H.; Sun, L.; Li, M.-Y.; Li, L.-J.; MacDonald, A. H.; Li, X. Direct measurement of exciton valley coherence in monolayer WSe_2. *Nat. Phys.* **2016**, *12*, 677−682.

(12) Chernikov, A.; Berkelbach, T. C.; Hill, H. M.; Rigosi, A.; Li, Y.; Aslan, O. B.; Reichman, D. R.; Hybertsen, M. S.; Heinz, T. F. Exciton binding energy and nonhydrogenic Rydberg series in monolayer WS_2. *Phys. Rev. Lett.* **2014**, *113*, 076802.

(13) Moody, G.; Dass, C. K.; Hao, K.; Chen, C.-H.; Li, L.-J.; Singh, A.; Tran, K.; Clark, G.; Xu, X.; Berghäuser, G.; Malic, E.; Li, X.; et al. Intrinsic homogeneous linewidth and broadening mechanisms of excitons in monolayer transition metal dichalcogenides. *Nat. Commun.* **2015**, *6*, 8315.

(14) Zhu, C.; Zhang, K.; Glazov, M.; Urbaszek, B.; Amand, T.; Ji, Z.; Liu, B.; Marie, X. Exciton valley dynamics probed by Kerr rotation in WSe_2 monolayers. *Phys. Rev. B: Condens. Matter Mater. Phys.* **2014**, *90*, 161302.

(15) Baranowski, M.; Surrente, A.; Maude, D.; Ballottin, M.; Mitioglu, A.; Christianen, P.; Kung, Y.; Dumcenco, D.; Kis, A.; Plochocka, P. Dark excitons and the elusive valley polarization in transition metal dichalcogenides. *2D Mater.* **2017**, *4*, 025016.

(16) Hong, X.; Kim, J.; Shi, S.-F.; Zhang, Y.; Jin, C.; Sun, Y.; Tongay, S.; Wu, J.; Zhang, Y.; Wang, F. Ultrafast charge transfer in atomically thin MoS_2/WS_2 heterostructures. *Nat. Nanotechnol.* **2014**, *9*, 682−686.

(17) Kang, J.; Tongay, S.; Zhou, J.; Li, J.; Wu, J. Band offsets and heterostructures of two-dimensional semiconductors. *Appl. Phys. Lett.* **2013**, *102*, 012111.

(18) Miller, B.; Steinhoff, A.; Pano, B.; Klein, J.; Jahnke, F.; Holleitner, A.; Wurstbauer, U. Long-lived direct and indirect interlayer excitons in van der Waals heterostructures. *Nano Lett.* **2017**, *17*, 5229−5237.

(19) Baranowski, M.; Surrente, A.; Klopotowski, L.; Urban, J.; Zhang, N.; Maude, D. K.; Wiwatowski, K.; Mackowski, S.; Kung, Y.-C.; Dumcenco, D.; Kis, A.; Plochocka, P. Probing the Interlayer Exciton Physics in a $MoS_2/MoSe_2/MoS_2$ van der Waals Heterostructure. *Nano Lett.* **2017**, *17*, 6360−6365.

(20) Rivera, P.; Seyler, K. L.; Yu, H.; Schaibley, J. R.; Yan, J.; Mandrus, D. G.; Yao, W.; Xu, X. Valley-polarized exciton dynamics in a 2D semiconductor heterostructure. *Science* **2016**, *351*, 688−691.

(21) Li, Y.; Ludwig, J.; Low, T.; Chernikov, A.; Cui, X.; Arefe, G.; Kim, Y. D.; van der Zande, A. M.; Rigosi, A.; Hill, H. M.; Kim, S. H.; Hone, J.; Li, Z.; Smirnov, D.; Heinz, T. F. Valley Splitting and Polarization by the Zeeman Effect in Monolayer $MoSe_2$. *Phys. Rev. Lett.* **2014**, *113*, 266804.

(22) Aivazian, G.; Gong, Z.; Jones, A. M.; Chu, R.-L.; Yan, J.; Mandrus, D. G.; Zhang, C.; Cobden, D.; Yao, W.; Xu, X. Magnetic control of valley pseudospin in monolayer WSe_2. *Nat. Phys.* **2015**, *11*, 148−152.

(23) Srivastava, A.; Sidler, M.; Allain, A. V.; Lembke, D. S.; Kis, A.; Imamoğlu, A. Valley Zeeman effect in elementary optical excitations of monolayer WSe_2. *Nat. Phys.* **2015**, *11*, 141−147.

(24) MacNeill, D.; Heikes, C.; Mak, K. F.; Anderson, Z.; Kormányos, A.; Zólyomi, V.; Park, J.; Ralph, D. C. Breaking of valley degeneracy by magnetic field in monolayer $MoSe_2$. *Phys. Rev. Lett.* **2015**, *114*, 037401.

(25) Mitioglu, A. A.; Plochocka, P.; del Águila, G.; Christianen, P. C. M.; Deligeorgis, G.; Anghel, S.; Kulyuk, L.; Maude, D. K. Optical Investigation of Monolayer and Bulk Tungsten Diselenide in High Magnetic Fields. *Nano Lett.* **2015**, *15*, 4387−4392.

(26) Nagler, P.; Ballottin, M. V.; Mitioglu, A. A.; Mooshammer, F.; Paradiso, N.; Strunk, C.; Huber, R.; Chernikov, A.; Christianen, P. C.; Schüller, C.; Korn, T. Giant magnetic splitting inducing near-unity valley polarization in van der Waals heterostructures. *Nat. Commun.* **2017**, *8*, 1551.

(27) Surrente, A.; Dumcenco, D.; Yang, Z.; Kuc, A.; Jing, Y.; Heine, T.; Kung, Y.-C.; Maude, D. K.; Kis, A.; Plochocka, P. Defect healing and charge transfer mediated valley polarization in $MoS_2/MoSe_2/MoS_2$ trilayer van der Waals heterostructures. *Nano Lett.* **2017**, *17*, 4130−4136.

(28) Zhang, C.; Chuu, C.-P.; Ren, X.; Li, M.-Y.; Li, L.-J.; Jin, C.; Chou, M.-Y.; Shih, C.-K. Interlayer couplings, Moiré patterns, and 2D electronic superlattices in MoS_2-WSe_2 hetero-bilayers. *Science Advances* **2017**, *3*, e1601459.

(29) Pan, Y.; Fölsch, S.; Nie, Y.; Waters, D.; Lin, Y.-C.; Jariwala, B.; Zhang, K.; Cho, K.; Robinson, J. A.; Feenstra, R. M. Quantum-Confined Electronic States arising from Moiré Pattern of MoS_2-WSe_2 Heterobilayers. *Nano Lett.* **2018**, *18*, 1849−1855.

(30) Kang, J.; Li, J.; Li, S.-S.; Xia, J.-B.; Wang, L.-W. Electronic structural Moiré pattern effects on $MoS_2/MoSe_2$ 2D heterostructures. *Nano Lett.* **2013**, *13*, 5485−5490.

(31) Yu, H.; Liu, G.-B.; Tang, J.; Xu, X.; Yao, W. Moiré excitons: From programmable quantum emitter arrays to spin-orbit-coupled artificial lattices. *Science Advances* **2017**, *3*, e1701696.

(32) Wu, F.; Lovorn, T.; MacDonald, A. Theory of optical absorption by interlayer excitons in transition metal dichalcogenide heterobilayers. *Phys. Rev. B: Condens. Matter Mater. Phys.* **2018**, *97*, 035306.

(33) Mouri, S.; Zhang, W.; Kozawa, D.; Miyauchi, Y.; Eda, G.; Matsuda, K. Thermal dissociation of inter-layer excitons in $MoS_2/MoSe_2$ hetero-bilayers. *Nanoscale* **2017**, *9*, 6674−6679.

(34) Raja, A.; Chaves, A.; Yu, J.; Arefe, G.; Hill, H. M.; Rigosi, A. F.; Berkelbach, T. C.; Nagler, P.; Schüller, C.; Korn, T.; Nuckolls, C.; Hone, J.; Brus, L. E.; Heinz, T. H.; Reichman, D. R.; Chernikov, A. Coulomb engineering of the bandgap and excitons in two-dimensional materials. *Nat. Commun.* **2017**, *8*, 15251.

(35) Stier, A. V.; Wilson, N. P.; Velizhanin, K. A.; Kono, J.; Xu, X.; Crooker, S. A. Magnetooptics of Exciton Rydberg States in a Monolayer Semiconductor. *Phys. Rev. Lett.* **2018**, *120*, 057405.

(36) Ramasubramaniam, A. Large excitonic effects in monolayers of molybdenum and tungsten dichalcogenides. *Phys. Rev. B: Condens. Matter Mater. Phys.* **2012**, *86*, 115409.

(37) Kormányos, A.; Burkard, G.; Gmitra, M.; Fabian, J.; Zólyomi, V.; Drummond, N. D.; Fal'ko, V. k· p theory for two-dimensional transition metal dichalcogenide semiconductors. *2D Mater.* **2015**, *2*, 022001.

DOI: 10.1021/acs.nanolett.8b01484
Nano Lett. XXXX, XXX, XXX−XXX

(38) Cao, T.; Wang, G.; Han, W.; Ye, H.; Zhu, C.; Shi, J.; Niu, Q.; Tan, P.; Liu, E. W. B.; Feng, J.; et al. Valley-selective circular dichroism of monolayer molybdenum disulphide. *Nat. Commun.* **2012**, *3*, 887.
(39) Zeng, H.; Dai, J.; Yao, W.; Xiao, D.; Cui, X. Valley Polarization in MoS_2 Monolayers by Optical Pumping. *Nat. Nanotechnol.* **2012**, *7*, 490.
(40) Aivazian, G.; Gong, Z.; Jones, A. M.; Chu, R.-L.; Yan, J.; Mandrus, D. G.; Zhang, C.; Cobden, D.; Yao, W.; Xu, X. Magnetic control of valley pseudospin in monolayer WSe_2. *Nat. Phys.* **2015**, *11*, 148.
(41) Neumann, A.; Lindlau, J.; Colombier, L.; Nutz, M.; Najmaei, S.; Lou, J.; Mohite, A. D.; Yamaguchi, H.; Högele, A. Opto-valleytronic imaging of atomically thin semiconductors. *Nat. Nanotechnol.* **2017**, *12*, 329−334.
(42) Blackwood, E.; Snelling, M. J.; Harley, R. T.; Andrews, S. R.; Foxon, C. T. B. Exchange interaction of excitons in GaAs heterostructures. *Phys. Rev. B: Condens. Matter Mater. Phys.* **1994**, *50*, 14246−14254.
(43) Worsley, R. E.; Traynor, N. J.; Grevatt, T.; Harley, R. T. Transient Linear Birefringence in GaAs Quantum Wells: Magnetic Field Dependence of Coherent Exciton Spin Dynamics. *Phys. Rev. Lett.* **1996**, *76*, 3224−3227.
(44) Glazov, M. M.; Amand, T.; Marie, X.; Lagarde, D.; Bouet, L.; Urbaszek, B. Exciton fine structure and spin decoherence in monolayers of transition metal dichalcogenides. *Phys. Rev. B: Condens. Matter Mater. Phys.* **2014**, *89*, 201302.
(45) Orbach, R. Spin-lattice relaxation in rare-earth salts. *Proc. R. Soc. London, Ser. A* **1961**, *264*, 458.
(46) Aksenov, I.; Aoyagi, Y.; Kusano, J.; Sugano, T.; Yasuda, T.; Segawa, Y. Temporal dynamics of a magnetoexciton in a quantum well. *Phys. Rev. B: Condens. Matter Mater. Phys.* **1995**, *52*, 17430−17434.
(47) Smoleński, T.; Kazimierczuk, T.; Goryca, M.; Molas, M. R.; Nogajewski, K.; Faugeras, C.; Potemski, M.; Kossacki, P. Magnetic field induced polarization enhancement in monolayers of tungsten dichalcogenides: effects of temperature. *2D Mater.* **2018**, *5*, 015023.
(48) Liu, G.-B.; Shan, W.-Y.; Yao, Y.; Yao, W.; Xiao, D. Three-band tight-binding model for monolayers of group-VIB transition metal dichalcogenides. *Phys. Rev. B: Condens. Matter Mater. Phys.* **2013**, *88*, 085433.
(49) Dumcenco, D.; Ovchinnikov, D.; Marinov, K.; Lazic, P.; Gibertini, M.; Marzari, N.; Sanchez, O. L.; Kung, Y.-C.; Krasnozhon, D.; Chen, M.-W.; Bertolazzi, S.; Gillet, P.; Fontcuberta i Morral, A.; Radenovic, A.; Kis, A. Large-area epitaxial monolayer MoS_2. *ACS Nano* **2015**, *9*, 4611−4620.
(50) Mitioglu, A.; Galkowski, K.; Surrente, A.; Klopotowski, L.; Dumcenco, D.; Kis, A.; Maude, D.; Plochocka, P. Magnetoexcitons in large area CVD-grown monolayer MoS_2 and $MoSe_2$ on sapphire. *Phys. Rev. B: Condens. Matter Mater. Phys.* **2016**, *93*, 165412.
(51) Wang, K.; Huang, B.; Tian, M.; Ceballos, F.; Lin, M.-W.; Mahjouri-Samani, M.; Boulesbaa, A.; Puretzky, A. A.; Rouleau, C. M.; Yoon, M.; Zhao, H.; Xiao, K.; Duscher, G.; Geohegan, D. B. Interlayer Coupling in Twisted WSe_2/WS_2 Bilayer Heterostructures Revealed by Optical Spectroscopy. *ACS Nano* **2016**, *10*, 6612−6622.

DOI: 10.1021/acs.nanolett.8b01484
Nano Lett. XXXX, XXX, XXX−XXX